

SUPPORTING INFORMATION

Polymorphs, phase transitions and stability in BaM₂(PO₄)₂ M = Mn, Fe, Co systems

Bastien Leclercq^a, Houria Kabbour^a, Angel Arevalo-Lopez^a, Marielle Huvé^a, Sylvie Daviero-Minaud^a, Claire Minaud^a, Ignacio Blazquez Alcover, Olivier Mentré^{a,*}

^a UCCS, UMR-CNRS 8181, Université Lille–ENSCL, Avenue Mendeleiev, 59655 Villeneuve d'Ascq, France

*Corresponding author: olivier.mentre@ensc-lille.fr

Table of Contents

(S1) Structural and powder refinement data for $\alpha\text{-BaFe}_2\text{P}_2\text{O}_8$	
Table S1a. Powder and refinement data for $\alpha\text{-BaFe}_2\text{P}_2\text{O}_8$ structure	S3
Table S1b. Atomic Positions & equivalent anisotropic thermal displacement for $\alpha\text{-BaFe}_2\text{P}_2\text{O}_8$	S3
(S2) Structural and powder refinement data for $\alpha\text{-BaMn}_2\text{P}_2\text{O}_8$ structure	
Table S2a. Powder and refinement data for $\alpha\text{-BaMn}_2\text{P}_2\text{O}_8$ structure	S4
Table S2b. Atomic Positions & equivalent anisotropic thermal displacement for $\alpha\text{-BaMn}_2\text{P}_2\text{O}_8$	S4
(S3) SEM EDS analysis	
Figure S3. SEM EDS analysis and resulting averaged atomic proportions (%)	S5
(S4) UV-Visible and IR spectroscopies	
Figure S4a. Transmittance Infrared and Absorbance UV Visible spectroscopies.....	S5
(S5) Thermal analysis for $\alpha\text{-BaFe}_2\text{P}_2\text{O}_8$ and $\alpha\text{-BaMn}_2\text{P}_2\text{O}_8$	
Figure S5a. Thermal stability for $\alpha\text{-BaFe}_2\text{P}_2\text{O}_8$ with DTA/ TGA measurement under flowing Argon, DTA/TGA measurement under flowing Air atmosphere, HTXRD evolution upon heating under flowing Nitrogen atmosphere	S6
Figure S5b. Thermal stability for $\alpha\text{-BaMn}_2\text{P}_2\text{O}_8$ with DTA under flowing Argon and Air atmosphere and HTXRD evolution ($\Delta T=50$ °C) upon heating under flowing Air atmosphere	S6
(S6) Cell parameters evolution and phase transformation upon heating for $\alpha\text{-BaFe}_2\text{P}_2\text{O}_8$ and $\alpha\text{- BaMn}_2\text{P}_2\text{O}_8$.	
Figure S6a. Cell parameters evolution upon heating under N2 atmosphere for $\alpha\text{-BaFe}_2\text{P}_2\text{O}_8$	S7
Figure S6b. Cell parameters evolution upon heating under N2 atmosphere for $\alpha\text{-BaMn}_2\text{P}_2\text{O}_8$	S7
(S7) Metastability in $\alpha\text{-BaFe}_2\text{P}_2\text{O}_8$	
Figure S7. $\alpha\text{-BaFe}_2\text{P}_2\text{O}_8$ to $\gamma\text{-BaFe}_2\text{P}_2\text{O}_8$ in one year at room temperature and pressure	S8
(S8) Phase transition in $\text{BaM}_2\text{P}_2\text{O}_8$ systems (M= Co, Fe, Mn)	
Table S8a. Phase transition in $\text{BaM}_2\text{P}_2\text{O}_8$ systems (M= Co, Fe, Mn) with corresponding crystallographic structure data.	S8
(S9) Synchrotron Diffraction data Refinement	
Figure S9. Synchrotron data refinement with (a) $\alpha\text{-BaFe}_2\text{P}_2\text{O}_8$ model refined (b) enlargement for $\alpha\text{-BaFe}_2\text{P}_2\text{O}_8$ (c) $\alpha\text{-BaMn}_2\text{P}_2\text{O}_8$ model refined and (d) relaxed DFT calculations model for $\alpha\text{-BaFe}_2\text{P}_2\text{O}_8$. against synchrotron data	S9
(S10) HTXRD vs relaxed model	
Figure S10. $\alpha\text{-BaFe}_2\text{P}_2\text{O}_8$ HTXRD between 30 °C and 501 °C	S9
(S11) Details about DFT calculations	
Table S11a. Comparison of system total Energy (in eV/FU) between $\alpha\text{-BaM}_2\text{P}_2\text{O}_8$ and $\gamma\text{-BaM}_2\text{P}_2\text{O}_8$ (M = Fe, Co, Mn) structure	S10
Table S11b. Refined and relaxed model comparison for $\alpha\text{-BaFe}_2\text{P}_2\text{O}_8$ and $\alpha\text{-BaMn}_2\text{P}_2\text{O}_8$	S11
Table S11c. Fe-O bond distances and associated Integral COHP for spins (\uparrow) and (\downarrow)	S12
(S12) Details about Orbitals representation for $\alpha\text{-BaFe}_2\text{P}_2\text{O}_8$	
Figure S12. 3D MO 3d Fe orbitals simulation with corresponding name and energies for $\alpha\text{-BaFe}_2\text{P}_2\text{O}_8$ structure	S12
(S13) Additional Magnetic Measurements	
Figure S13. Magnetic measurements data for $\alpha\text{-BaFe}_2\text{P}_2\text{O}_8$ and $\alpha\text{-BaMn}_2\text{P}_2\text{O}_8$	S13
(S14) Specific Heat measurement	
Figure S14. $\alpha\text{-BaFe}_2\text{P}_2\text{O}_8$ specific heat measurement	S13
(S15) Powder Neutron Diffraction refinement	
Figure S14. $\alpha\text{-BaMn}_2\text{P}_2\text{O}_8$ and $\alpha\text{-BaFe}_2\text{P}_2\text{O}_8$ PND Rietveld refinement at 80K.....	S14

(S1) Structural and powder refinement data for α -BaFe₂P₂O₈

Table S1a. Powder and refinement data for α -BaFe₂P₂O₈ structure.

Powder Data (T=293K)	
Formula	α -BaFe ₂ P ₂ O ₈
Molar weight (g/mol)	438,968
Symmetry	Trigonal
Space group	P 3 ₁ 2 1 (152)
Unit cell (Å) and angle (°)	a = 5,114124(14) c = 25,11130(8)
Volume (Å ³)	568,777(3)
Z	3
Data collection	
Equipment	Synchrotron (111-DIAMOND)
λ (K α ; Å)	0,824899
Sample Holder	0,5mm Glass Capillary
density calc. (g/cm ³)	3,8448
Sample	Powder
Color	grey
θ (min-max) (°)	2,10800 - 92,11200
μ (mm ⁻¹ for λ (K α =0,824899Å))	13,884
R _{Bragg} (%)	6,629

Table S1b. Atomic Positions & equivalent anisotropic thermal displacement for α -BaFe₂P₂O₈ structure.

Atom	Wick.	x	y	z	Ueq (Å ²)
Ba1	3a	0,04080(15)	0,000000	0,33333	0,00291(8)
Fe1	6c	0,6849(6)	0,2596(5)	0,21819(7)	0,0274(6)
P1	6c	0,6547(7)	0,3408(6)	0,08844(9)	0,0519(9)
O1	6c	0,7176(11)	0,4602(10)	0,14559(12)	0,0550(14)
O2	6c	0,8988(9)	0,5303(10)	0,05088(18)	0,0550(14)
O3	6c	0,5843(11)	0,0073(7)	0,08565(18)	0,0550(14)
O4	6c	0,3471(8)	0,3197(11)	0,07184(18)	0,0550(14)

(S2) Structural and powder refinement data for α -BaMn₂P₂O₈ structure

Table S2a. Powder and refinement data for α -BaMn₂P₂O₈ structure.

Powder Data (T=293K)	
Formula	α -BaMn ₂ P ₂ O ₈
Molar weight (g/mol)	437,15
Symmetry	Monoclinic
Space group	C 1 2 1 (5)
Unit cell (Å) and angle (°)	a = 9.09710(4) b=5.18068(2) c = 24.98384(12)
β (°)	90.4107(2)
Volume (Å ³)	1177.437(9)
Z	6
Data collection	
Equipment	Synchrotron (I11-DIAMOND)
λ (K α ; Å)	0,824899
Sample Holder	0,5mm Glass Capillary
density calc. (g/cm ³)	3,6991
Sample	Powder
Color	Pale Pink
θ (min-max) (°)	2,10800 - 92,11200
μ (mm ⁻¹ for λ (K α =0,824899Å))	12,695
R _{Bragg} (%)	10,9

Table S2b. Atomic Positions & equivalent anisotropic thermal displacement for α -BaMn₂P₂O₈ structure.

Atom	Wick.	x	y	z	Ueq (Å ²)
Ba1	4c	0.02273(18)	0.0502(8)	0.33372(9)	0.0218(5)
Ba2	2a	0.00000	0.0520(10)	0.00000	0.0407(10)
Mn1	4c	-0.2804(4)	0.0571(11)	0.21869(14)	0.0063(4)
Mn2	4c	-0.1187(4)	-0.4549(14)	0.11200(15)	0.0063(4)
Mn3	4c	0.1616(5)	-0.3240(9)	0.5545(2)	0.0063(4)
P1	4c	0.1586(4)	0.5793(8)	0.08829(15)	0.041(3)
O1_1	4c	0.1079(7)	0.5545(13)	0.14692(13)	0.054(3)
O2_1	4c	0.1843(7)	0.8602(6)	0.0748(3)	0.054(3)
O3_1	4c	0.3013(5)	0.4229(11)	0.0820(3)	0.054(3)
O4_1	4c	0.0399(5)	0.4629(12)	0.0519(2)	0.054(3)
P2	4c	-0.1444(4)	-0.4690(8)	0.24836(15)	0.015(2)
O1_2	4c	-0.2070(6)	-0.5375(12)	0.19245(15)	0.004(2)
O2_2	4c	-0.2251(6)	-0.6320(11)	0.2898(2)	0.004(2)
O3_2	4c	0.0210(3)	-0.5347(12)	0.2502(2)	0.004(2)
O4_2	4c	-0.1619(6)	-0.1895(6)	0.2598(2)	0.004(2)
P3	4c	0.3348(4)	0.0933(7)	0.58069(14)	0.003(2)
O1_3	4c	0.3464(7)	-0.0107(12)	0.52385(14)	0.046(3)
O2_3	4c	0.4707(5)	0.0186(13)	0.6132(2)	0.046(3)
O3_3	4c	0.3144(7)	0.3860(6)	0.5805(3)	0.046(3)
O4_3	4c	0.1976(5)	-0.0266(12)	0.6071(2)	0.046(3)

(S3) SEM EDS analysis

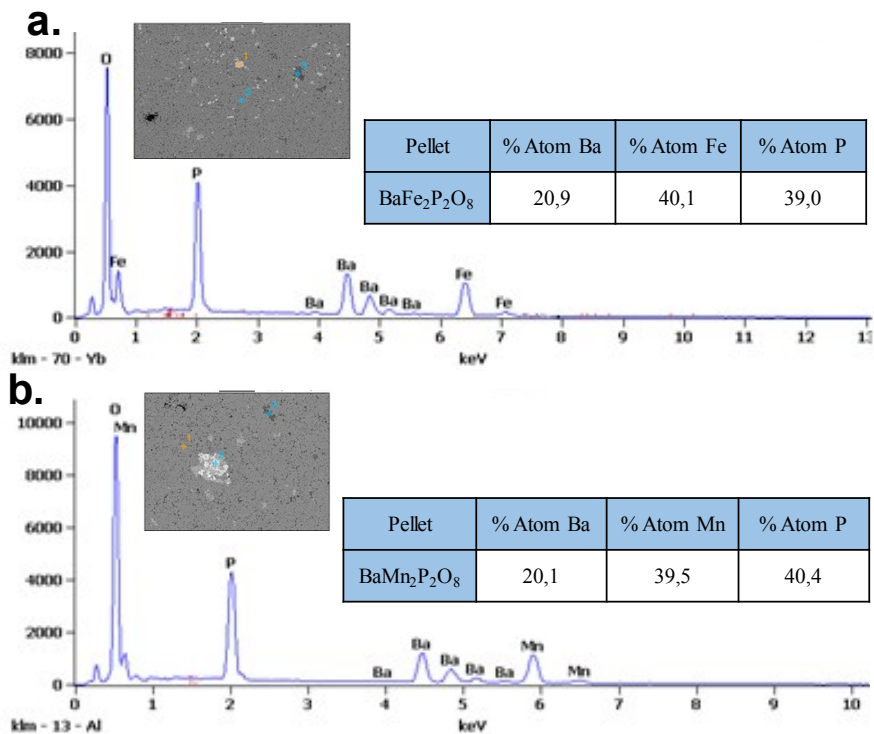


Figure S3. SEM EDS analysis and resulting averaged atomic proportions (%) performed on (a) $\alpha\text{-BaFe}_2\text{P}_2\text{O}_8$ pellet and (b) $\alpha\text{-BaMn}_2\text{P}_2\text{O}_8$ pellet.

(S4) UV-Visible and IR spectroscopies

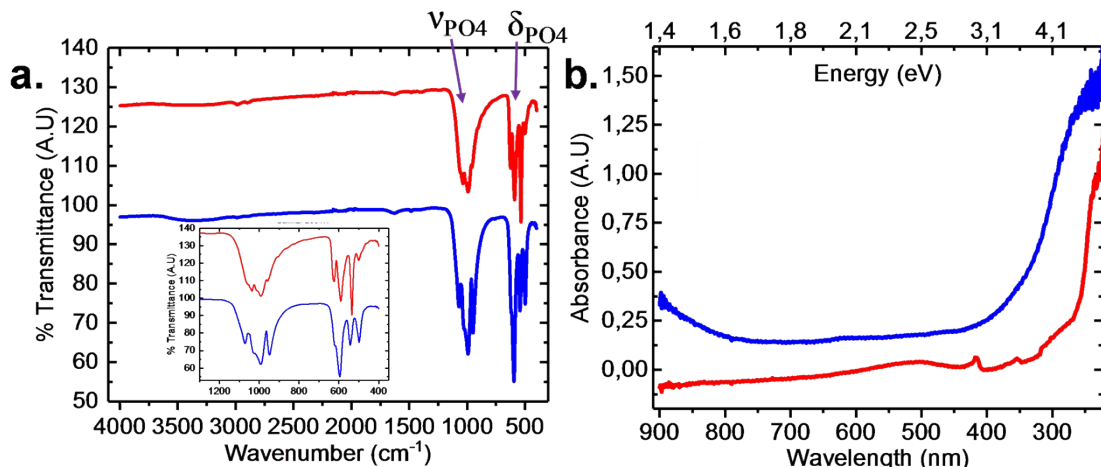


Figure S4. (a) Transmittance Infrared Spectra ofr $\alpha\text{-BaFe}_2\text{P}_2\text{O}_8$ (in blue) and $\alpha\text{-BaMn}_2\text{P}_2\text{O}_8$ (in red). The IR spectra show only evidence of stretching and bending PO_4 vibrations bands. Respectively ($1062 \text{ cm}^{-1}, 1039 \text{ cm}^{-1}, 996 \text{ cm}^{-1}, 955 \text{ cm}^{-1} // 627 \text{ cm}^{-1}, 593 \text{ cm}^{-1}, 534 \text{ cm}^{-1}, 499 \text{ cm}^{-1}$) for $\alpha\text{-BaMn}_2\text{P}_2\text{O}_8$ and ($1074 \text{ cm}^{-1}, 1029 \text{ cm}^{-1}, 996 \text{ cm}^{-1}, 950 \text{ cm}^{-1} / 622 \text{ cm}^{-1}, 593 \text{ cm}^{-1}, 540 \text{ cm}^{-1}, 499 \text{ cm}^{-1}$) for $\alpha\text{-BaFe}_2\text{P}_2\text{O}_8$. (b) Absorbance UV Visible spectroscopies for $\alpha\text{-BaFe}_2\text{P}_2\text{O}_8$ (in blue) and $\alpha\text{-BaMn}_2\text{P}_2\text{O}_8$ (in red). Broad transition around 550 nm responsible for the pink shade of the $\alpha\text{-BaMn}_2\text{P}_2\text{O}_8$ compound.

(S5) Thermal analysis for $\alpha\text{-BaFe}_2\text{P}_2\text{O}_8$ and $\alpha\text{-BaMn}_2\text{P}_2\text{O}_8$

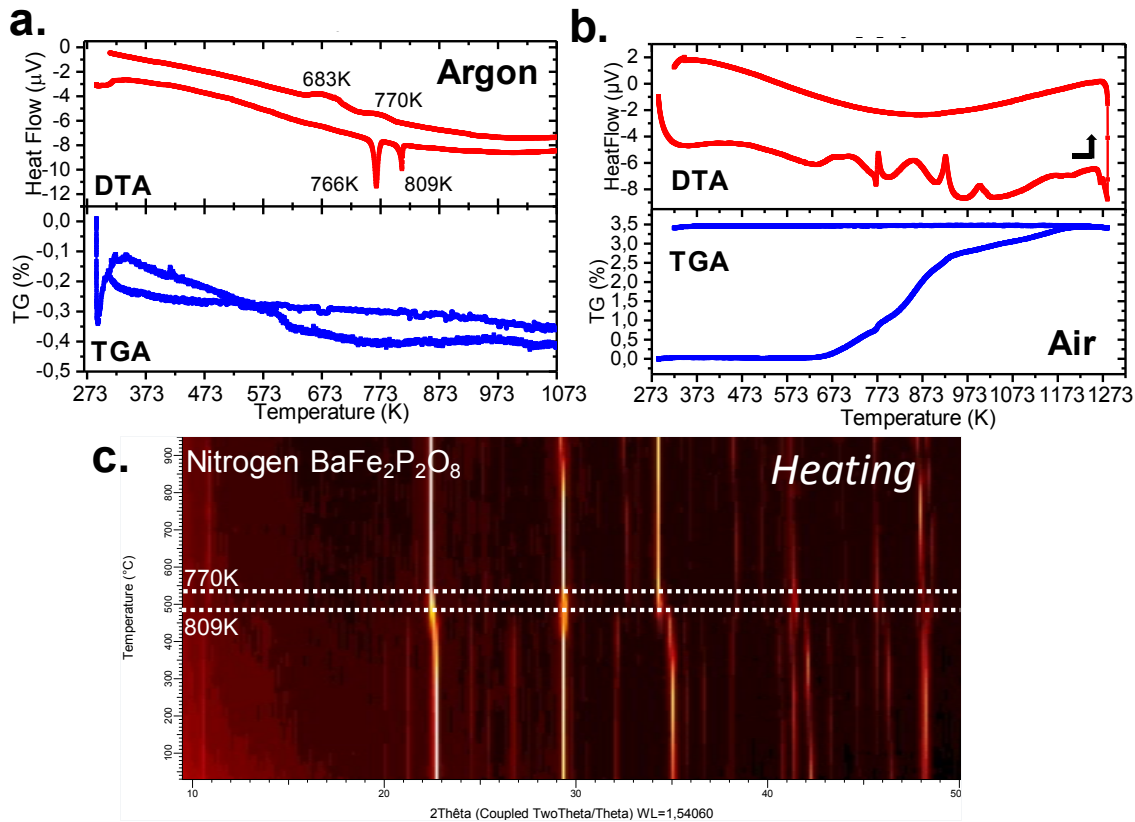


Figure S5a. Thermal stability for α -BaFe₂P₂O₈ with (a) DTA and corresponding TGA measurement under flowing Argon atmosphere (red and blue respectively), with highlighting of the two transformation $\alpha \rightarrow \alpha'$ (766 K), $\alpha' \rightarrow \beta$ (809 K) and reversibility. No weigh loss along the measurement. (b) DTA and TGA measurement under flowing Air atmosphere (red and blue respectively). The structure decomposes. We notice a weight gain corresponding to the decomposition of the structure, result of iron oxidation. (c) HTXRD evolution ($\Delta T=50$ K) upon heating under flowing Nitrogen atmosphere with evidence of the two transformation. Reversibility of transformations were also checked upon cooling.

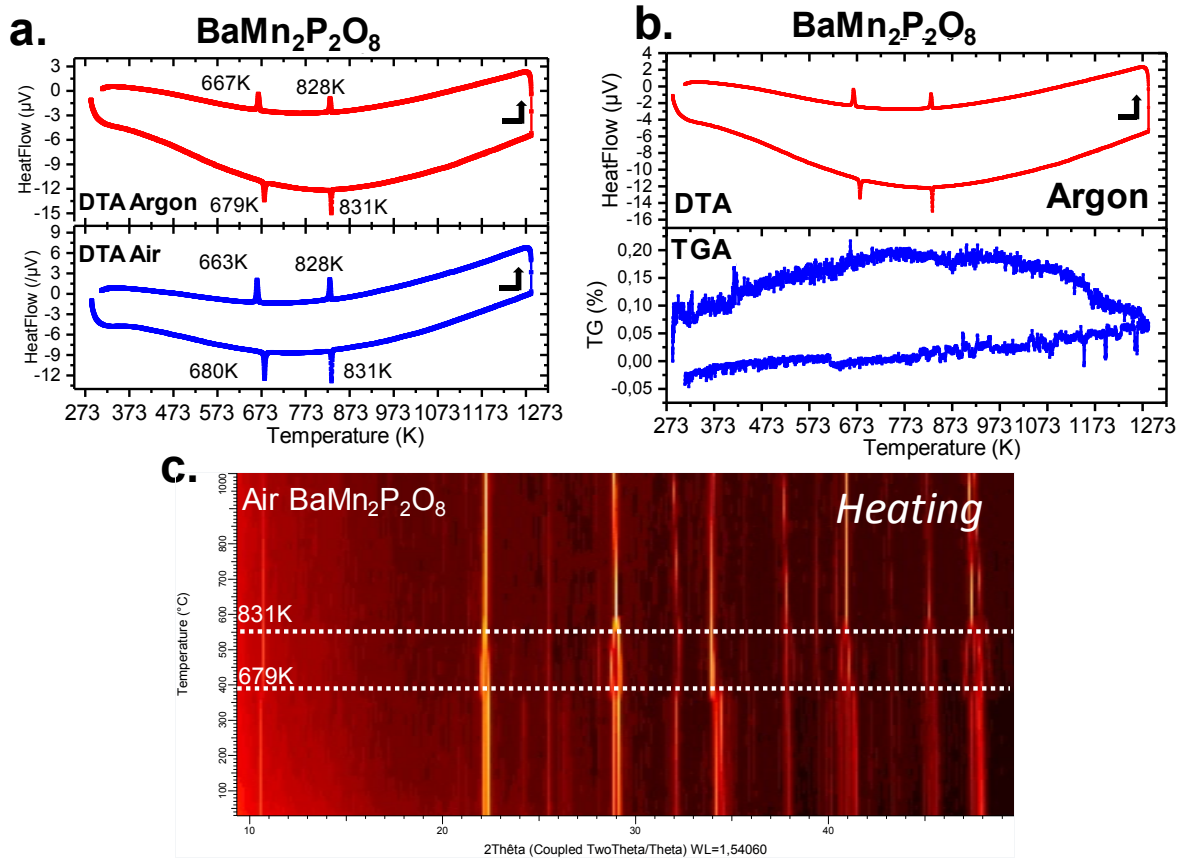


Figure S5b. Thermal stability for $\alpha\text{-BaMn}_2\text{P}_2\text{O}_8$ with (a) DTA under flowing Argon atmosphere (red) and DTA under flowing Air atmosphere (blue), with highlighting of the two transformation $\alpha \rightarrow \alpha'$ (679 K) and $\alpha' \rightarrow \beta$ (831 K) and reversibility upon cooling. (b) DTA and TGA measurement under flowing Argon atmosphere (red and blue respectively). No weight loss upon the measurement. (c) HTXRD evolution ($\Delta T=50$ K) upon heating under flowing Air atmosphere with evidence of the two transformation. Reversibility of transformations were also checked upon cooling.

(S6) Cell parameters evolution and phase transformation upon heating for $\alpha\text{-BaFe}_2\text{P}_2\text{O}_8$ and $\alpha\text{-BaMn}_2\text{P}_2\text{O}_8$.

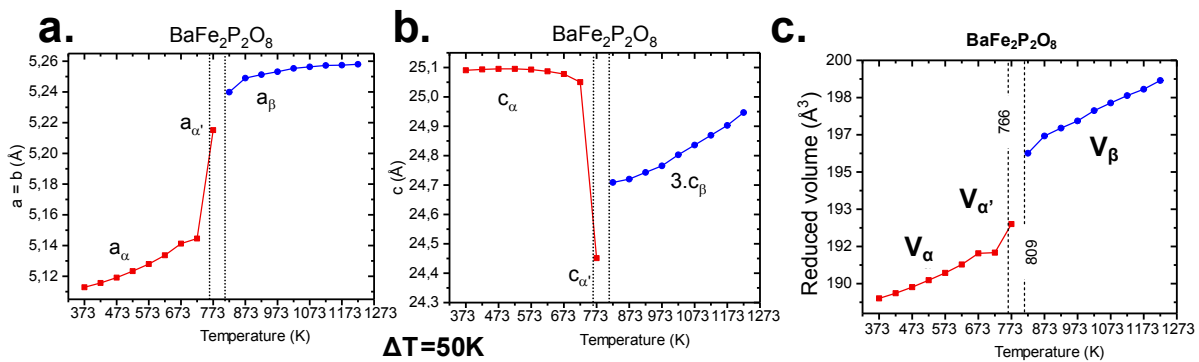


Figure S6a. Cell parameters evolution upon heating under nitrogen atmosphere for $\alpha\text{-BaFe}_2\text{P}_2\text{O}_8$ with (a) a parameter evolution (\AA), (b) c parameter evolution (\AA) and (c) reduced volume evolution (\AA^3). Values obtained from “le Bail” refinement of previous HTXRD datas ($\Delta T=50$ K).

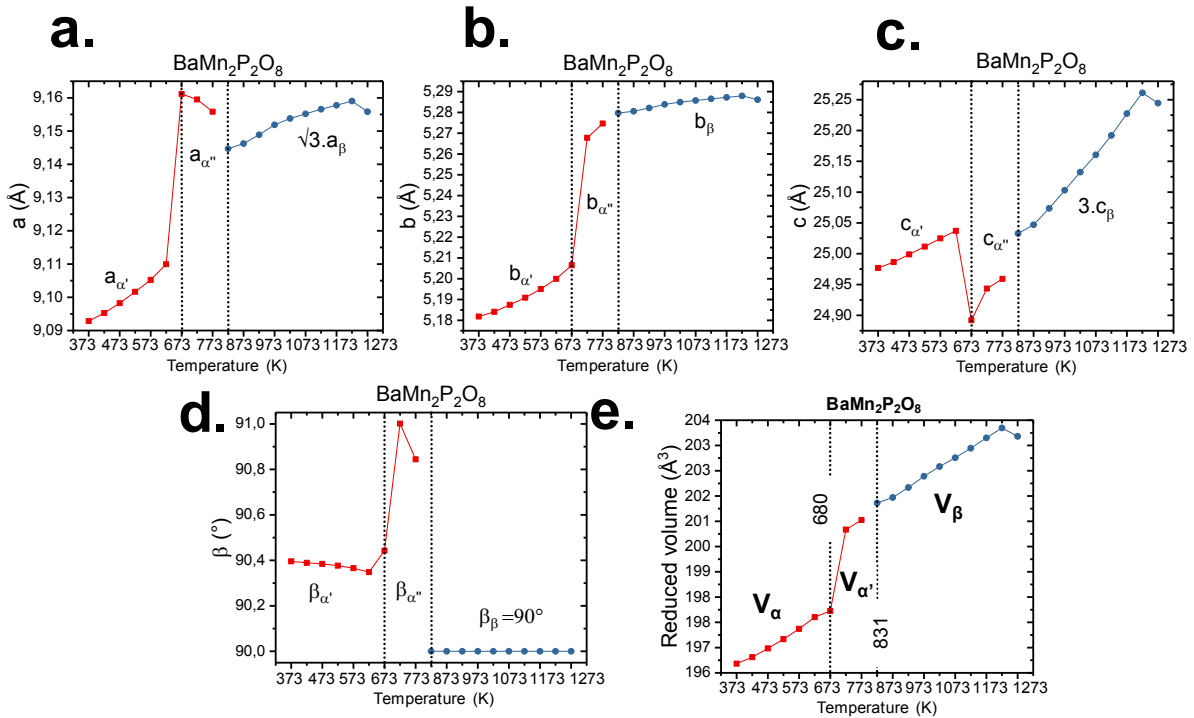
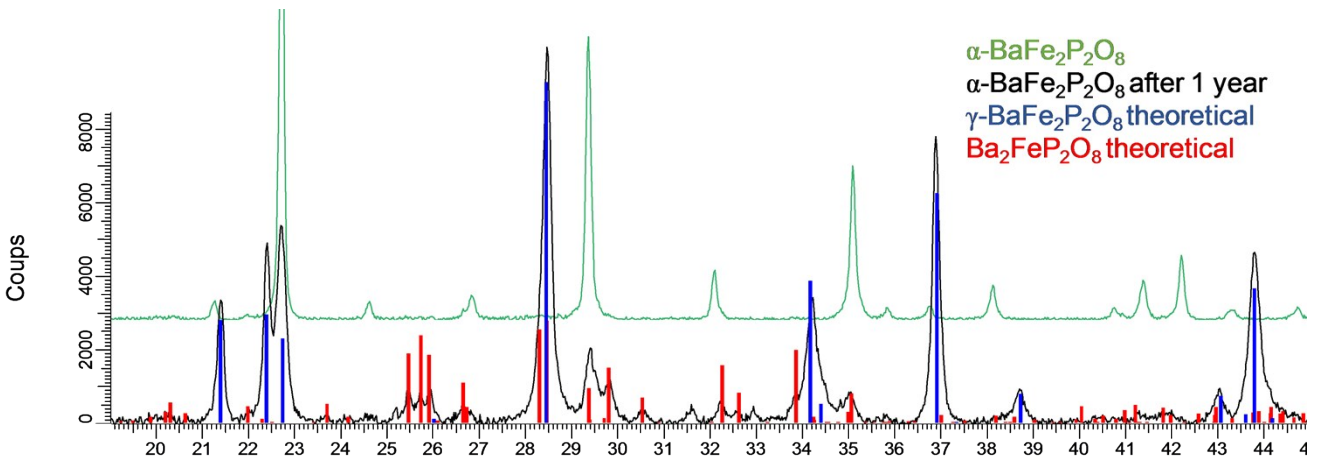


Figure S6b. Cell parameters evolution from monoclinic (in red) to trigonal structure (in blue) upon heating under nitrogen atmosphere for $\alpha\text{-BaMn}_2\text{P}_2\text{O}_8$ with (a) a parameter evolution (\AA), (b) b parameter evolution (\AA), (c) c parameter evolution (\AA), (d) β parameter evolution ($^{\circ}$) and (e) reduced volume evolution (\AA^3). Values obtained from “le Bail” refinement of HTXRD datas ($\Delta T=50$ K).



(S7) Metastability in $\alpha\text{-BaFe}_2\text{P}_2\text{O}_8$

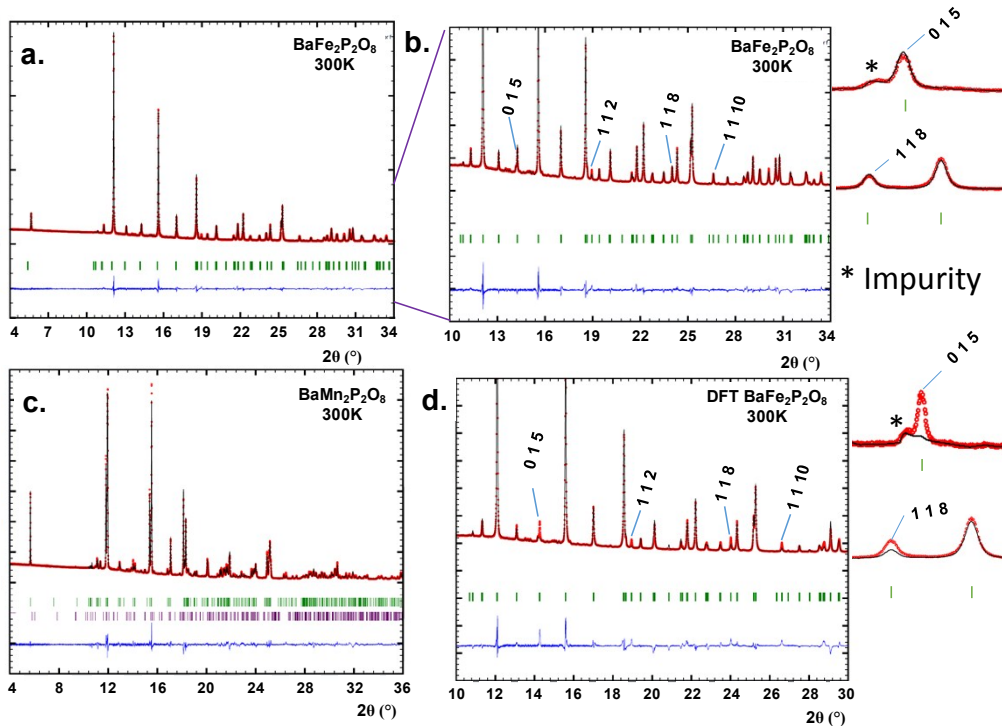
Figure S7. $\alpha\text{-BaFe}_2\text{P}_2\text{O}_8$ to $\gamma\text{-BaFe}_2\text{P}_2\text{O}_8$ in one year at room temperature and pressure. “Fresh” $\alpha\text{-BaFe}_2\text{P}_2\text{O}_8$ experimental diagram show in green, “1-year-old” $\alpha\text{-BaFe}_2\text{P}_2\text{O}_8$ experimental diagram in black, theoretical $\gamma\text{-BaFe}_2\text{P}_2\text{O}_8$ in blue, and theoretical $\text{Ba}_2\text{FeP}_2\text{O}_8$ in red.

(S8) Phase transition in $\text{BaM}_2\text{P}_2\text{O}_8$ systems ($M=\text{Co, Fe, Mn}$)

Table S8a. Sum up table for phase transition in $\text{BaM}_2\text{P}_2\text{O}_8$ systems ($M=\text{Co, Fe, Mn}$) with corresponding details about crystallographic structure data.

		T °K	S.G.	Z	a (Å)	b (Å)	c (Å)	β (°)	Volume (Å³)	ρ (g/cm³)
BaCo₂P₂O₈	α	293	P21/a	2	9,2110(3)	5,0040(2)	8,0851(3)	92,7370(10)	372,23	3,97
	α'	-	-	-	-	-	-	-	-	-
	α''	873	P21/a	2	8.2395(6)	5.1739(4)	9.0055(5)	91.155(3)	383.83	3.85
	β	1173	P-3	1	5,22264(4)	5,22264(4)	8,26062(10)	90	195,13	3,79
	γ	298	R-3	3	4,8554(6)	4,8554(6)	23,2156(17)	90	473,98	4,68
	ε		P21/c					Magnetic, Resistivity, dielectric transitions		
BaFe₂P₂O₈	α	293	P3_121	3	5,1140(1)	5,1140(1)	25,1108(1)	90	568,75	3,84
	α'	773	P3_121	3	5,2151(3)	5,2151(3)	24,4512(4)	90	578,01	3,78
	β	1173	P-3	1	5,2580(2)	5,2580(2)	8,3156(5)	90	199,10	3,66
	γ	293	R-3	3	4,8730(2)	4,8730(2)	23,368(2)	90	480,56	4,55
	γ'	100	P-1	1	4,8656(8)	4,8584(8)	8,2481(11)	106,850(7) 107,012(7) 60,333(7)	159,52	4,57
BaMn₂P₂O₈	HP	293	P21/a	2	9,2830(12)	4,9783(6)	8,1326(10)	94,106(7)	374,87	3,87
	α	293	C2	6	9,09740(1)	5,1808(1)	24,9849(1)	90,4112(2)	1177,55	3,70
	α'	773	C2	6	9,1558(3)	5,2747(2)	24,9592(3)	90,8443(2)	1205,25	3,61
	β	1273	P-3	1	5,2861(3)	5,2861(3)	8,4148(5)	90	203,63(2)	3,56

(S9)



Synchrotron Diffraction data Refinement

Figure S9. Synchrotron data refinement with (a) α - $\text{BaFe}_2\text{P}_2\text{O}_8$ model refined (b) enlargement for α - $\text{BaFe}_2\text{P}_2\text{O}_8$ (c) α - $\text{BaMn}_2\text{P}_2\text{O}_8$ model refined and (d) relaxed DFT calculations model for α - $\text{BaFe}_2\text{P}_2\text{O}_8$ on experimental synchrotron data. In the latter, the missing intensities (in particular 015 and 118) are highlighted on the right. The green mark corresponds to the alpha phase, the purple to the $\text{Ba}_2\text{MnP}_2\text{O}_8$ impurities refined in the case of α - $\text{BaMn}_2\text{P}_2\text{O}_8$ but excluded in the case of α - $\text{BaFe}_2\text{P}_2\text{O}_8$ (we were not able to refine it properly).

(S10) HTXRD vs relaxed model

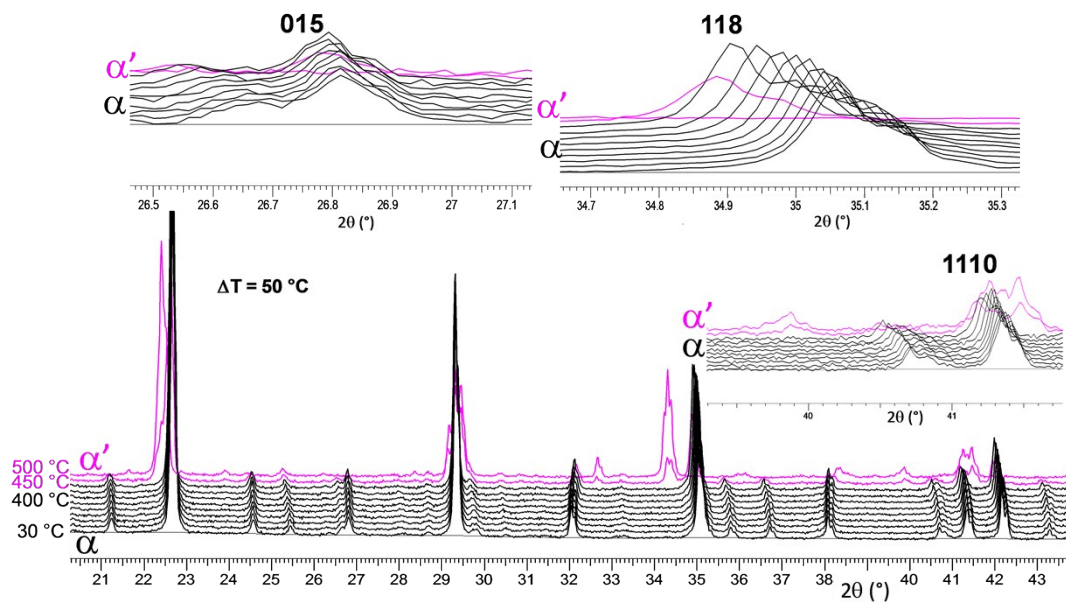


Figure S10. α - $\text{BaFe}_2\text{P}_2\text{O}_8$ HTXRD between 30 °C and 501 °C. From 30 to 400°C we're in the alpha form (black lines), from 400 °C to 501 °C (magenta lines) we're in the alpha' form. In the latter, we see loss in intensity on characteristic peaks in agreement with the relaxed structure model from DFT.

(S11) Details about DFT calculations

Table S11a. Comparison of system total Energy (in eV/FU) between α -BaM₂P₂O₈ and γ -BaM₂P₂O₈ ($M = Fe, Co, Mn$) structure. We used our refined model from synchrotron data for α -BaFe₂P₂O₈ and α -BaMn₂P₂O₈, and ICSD structure for the others. On the upper part of the tables, only the non-coherent γ -BaMn₂P₂O₈ structure was fully relaxed, starting from the closest γ -BaCo₂P₂O₈ structure. On the bottom part, values for the relaxed α -BaFe₂P₂O₈ and γ -BaFe₂P₂O₈, cell parameters and volume constant.

System	Structure	U and k points mesh	Total Energy (eV/FU)	Difference (eV/FU)
BaFe ₂ P ₂ O ₈	α , P3 ₁ 21	U= 6 eV 10x10x2 k mesh (104 k points)	-90,118	0,850
	γ , R-3	U= 6 eV 12x12x2 k mesh (52 k points)	-90,968	
BaCo ₂ P ₂ O ₈	α , P21/a	U = 4 eV 6x10x8 k mesh (244 k points)	-90,885	-1,070
	γ , R-3	U = 4 eV 12x12x2 k mesh (52 k points)	-89,814	
BaMn ₂ P ₂ O ₈	α , C2	U = 4 eV 2x5x1 k mesh (44 k points)	-97,002	-1,012
	γ , R-3	U = 4 eV 6x6x1 k mesh after full relaxation	-95,990	
After relaxations with unit cell parameters constrained				
BaFe ₂ P ₂ O ₈	α , P3 ₁ 21	U= 6 eV 10x10x2 k mesh (104 k points)	-92,610	-1,623
	γ , R-3	U= 6 eV 6x6x1 k mesh (8 k points)	-90,986	

Table S11b. To the left, comparison of Fe-O and P-O distances between refined α -BaFe₂P₂O₈ model from the synchrotron data, and relaxed α -BaFe₂P₂O₈ model from DFT calculations. To the right, comparison of Fe-O and P-O distances between refined α -BaMn₂P₂O₈ model from the synchrotron data, and relaxed α -BaMn₂P₂O₈ model from DFT calculations.

α -BaFe ₂ P ₂ O ₈	Refined	DFT	α -BaMn ₂ P ₂ O ₈	Refined Mn	DFT	α -BaMn ₂ P ₂ O ₈	Refined P	DFT P
Fe-O1 (Å)	2,057(4)	1,947	Mn1—O1_1 (Å)	2.055(5)	1,943	P1—O1_1 (Å)	1.544(5)	1,610
Fe-O1 (Å)	2,524(6)	1,984	Mn1—O1_2 (Å)	2.301(8)	1,976	P1—O2_1 (Å)	1.512(5)	1,553(3)
Fe-O3 (Å)	2,072(4)	2,022	Mn1—O2_2 (Å)	2.448(7)	2,125	P1—O3_1 (Å)	1.539(6)	1,540
Fe-O2 (Å)	2,589(6)	2,028	Mn1—O3_2 (Å)	2.032(5)	2,053	P1—O4_1 (Å)	1.530(6)	1,565
Fe-O4 (Å)	1,767(4)	2,032	Mn1—O4_2 (Å)	1.958(6)	2,054		5,04(4)	4,43
Fe-P (Å)	2,641(5)	2,601		2,06(2)	2,66	P2—O1_2 (Å)	1.546(6)	1,612
Fe-P (Å)	3,041(4)	3,171	Mn2—O1_1 (Å)	2.233(7)	1,997	P2—O2_2 (Å)	1.528(7)	1,567
Fe-P (Å)	3,298(4)	3,185	Mn2—O2_1 (Å)	2.229(8)	2,067	P2—O3_2 (Å)	1.543(5)	1,554
	1,99(2)	2,43	Mn2—O3_1 (Å)	2.217(9)	2,072	P2—O4_2 (Å)	1.485(5)	1,563
P1-O3 (Å)	1,559(5)	1,539	Mn2—O4_1 (Å)	2.133(6)	2,098		5,13(4)	4,43
P1-O2 (Å)	1,476(6)	1,553	Mn2—O1_2 (Å)	2.212(6)	1,937	P3—O1_3 (Å)	1.523(5)	1,613
P1-O4 (Å)	1,578(7)	1,568		1,64(2)	2,62	P3—O2_3 (Å)	1.524(6)	1,551
P1-O1 (Å)	1,530(4)	1,596	Mn3—O1_3 (Å)	2.463(8)	1,968	P3—O3_3 (Å)	1.528(5)	1,536
	4,84(3)	4,46	Mn3—O1_3 (Å)	2.184(6)	1,943	P3—O4_3 (Å)	1.546(6)	1,572
			Mn3—O2_3 (Å)	2.422(7)	2,087		5,06(4)	4,42
			Mn3—O3_3 (Å)	2.144(7)	2,060			
			Mn3—O4_3 (Å)	2.050(7)	2,124			
					1,60(2)	2,62		

Table S11c. Fe-O bond distances and associated Integral COHP for spins (\uparrow) and (\downarrow), negative values of ICOHP are indicating net bonding character.

Bond	Distance (Å)	ICOHP spin (\uparrow) (eV)	ICOHP spin (\downarrow) (eV)
Fe1-O	1.767	-1.04414	-1.62688
Fe1-O	2.057	-1.00795	-1.21956
Fe1-O	2.072	-0.89122	-1.09690
Fe1-O	2.524	-0.84155	-0.93160
Fe1-O	2.589	-0.54278	-0.62248

(S12) Details about Orbitals representation for $\alpha\text{-BaFe}_2\text{P}_2\text{O}_8$.

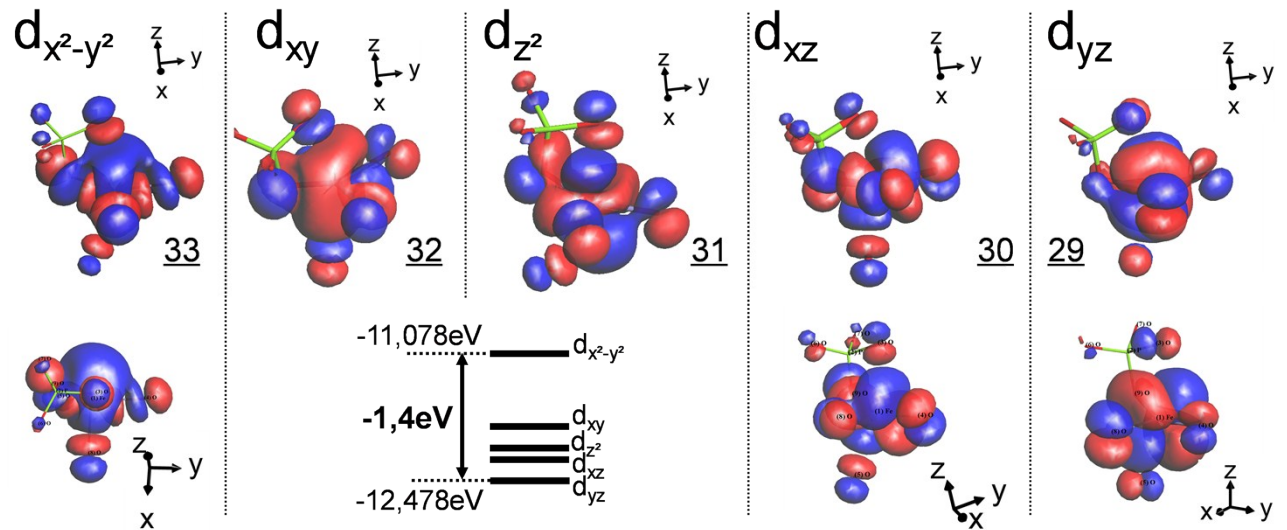


Figure S12. 3D MO d Fe orbitals simulation with corresponding name and energies for $\alpha\text{-BaFe}_2\text{P}_2\text{O}_8$ structure.

(S13) Additional Magnetic Measurements

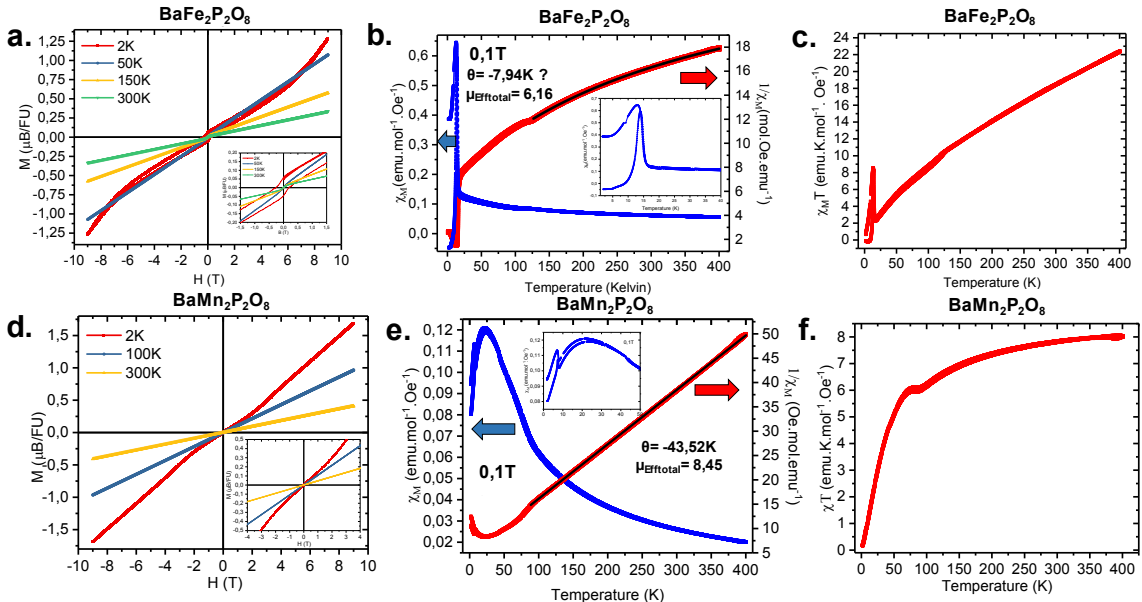


Figure S13. Magnetic measurements data for α -BaFe₂P₂O₈ with (a) MvsH at 2 K, 50 K, 150 K, 300 K, between -9 T and 9 T(b) ZFC/FC χ_M and $1/\chi_M$, blue and red respectively) from 400 K to 2K, and (c) corresponding $\chi_M T$. We recall the presence of Fe₃O₄ impurities in the sample, proved by the Verwey phase transition at 125 K. Magnetic measurements data for α -BaMn₂P₂O₈ with (d) MvsH at 2 K, 100 K, 300 K, between -9 T and 9 T (b) ZFC/FC χ_M and $1/\chi_M$, blue and red respectively) from 400 K to 2K, and (c) corresponding $\chi_M T$.

(S14) Specific Heat measurement

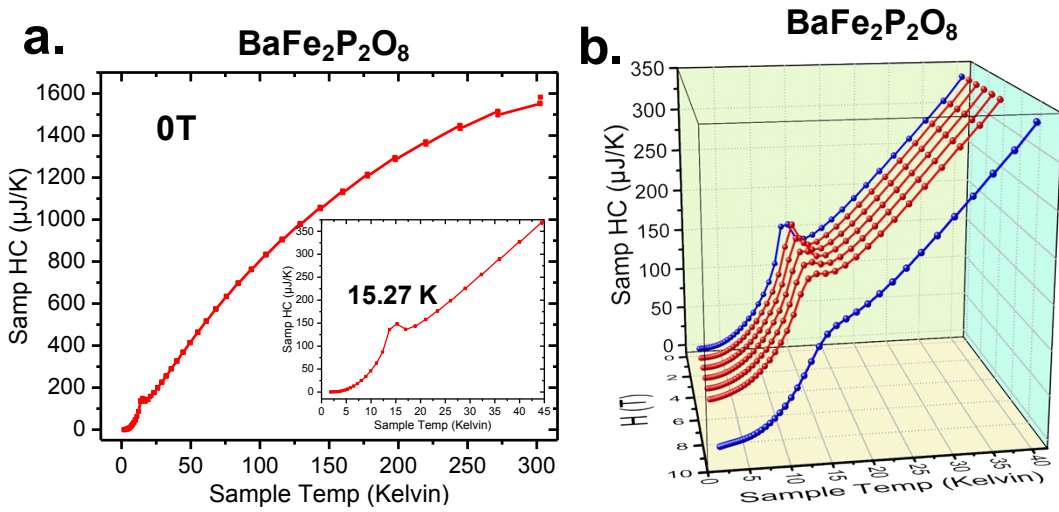


Figure S14. (a) α -BaFe₂P₂O₈ specific heat measurement between 300 K and 2K at 0 T, (b) α -BaFe₂P₂O₈ specific heat measurement between 40 K and 2K under different field from 0 to 9 T.

(S15) Powder Neutron Diffraction refinement

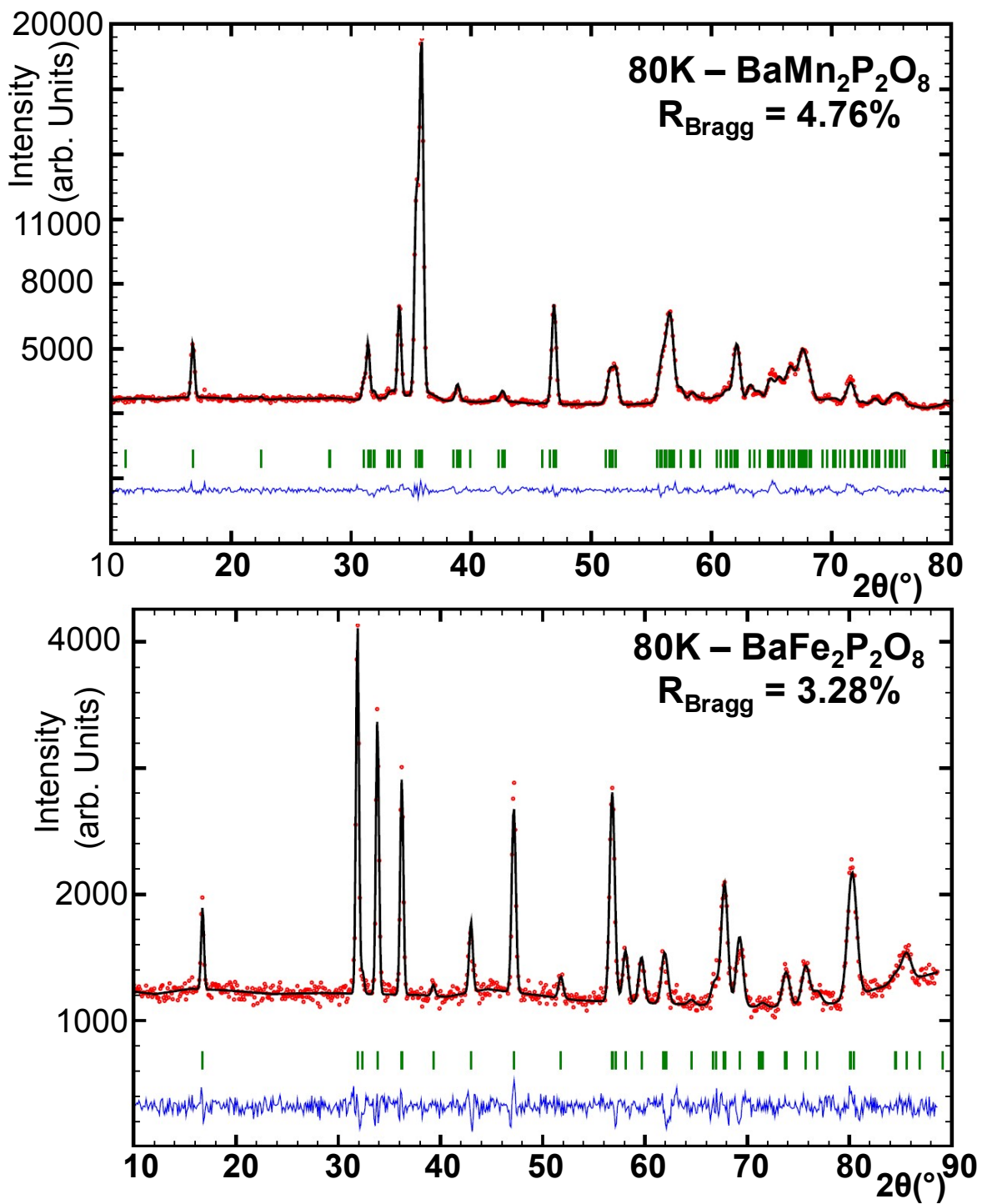


Figure S15. α -BaMn₂P₂O₈ and α -BaFe₂P₂O₈ powder neutron diffraction Rietveld refinement (a and b respectively) at 80K with our synchrotron refined model. The green mark corresponds to Bragg peaks, the red curves to the experimental measured points, the black curves to the intensity following our model, and the blue curves to the difference between them. At 80 K we are above the T_N of both compounds (so there is only structural contribution to the intensities measured).